Efficient experimental and numerical methods for solving vertical distribution of sediments in dam-break flows

Thomas Rowan and Mohammed Seaid

Abstract In this work, a class of efficient experimental and numerical methods for recording sediment distributions in dam-break flows is developed and assessed. A new experimental platform is developed and tested enabling accuracy and high frame-per-second images to be generated and evaluated. The novelty of this study is that the collected images are broken down into smaller cellular based images which are individually assessed for their color contents. Every frame collected is first filtered to exclude any background pixels and remove the effects of photography and lighting, then the color spectra of the frame is analyzed and sensible filtering added to remove the complex effects of fluid features including ripples and air bubbles. Once these processes are complete, a simple color comparison can be utilized to assess the sediment fraction of the flow in each frame and cell. The proposed method is used on a small-scale dam-break problem and a four-stage breakdown of the dam-break is given with measured sediment levels accounted for. Mathematical models based on multilayer shallow water equations with mass exchange terms are developed in this study. The governing equations form a system of conservation laws with source terms. As numerical methods we implement a fast, accurate and well-balanced finite volume characteristics solver. Comparisons between experimental and numerical results for the vertical distribution of sediments in a dam-break problem are also discussed.

Thomas Rowan
Department of Civil and Environmental Engineering, Imperial College London, South Kensington Campus, London SW72AZ, UK. e-mail: t.rowan@imperial.ac.uk

Mohammed Seaid
Department of Engineering, University of Durham, South Road, Durham DH1 3LE, UK. e-mail: m.seaid@durham.ac.uk

1 Introduction

Transport of sediments is a crucial aspect of modeling sedimentary flows, although it is very hard to know exactly what mode of sediment transport is prevalent in any flow. In general there are five modes of sediment transport; dissolved load, wash load, suspended load, intermittently suspended (or bounding) load, and bed load. Often the former three and latter two are amalgamated to give suspended and bed load, see for instance [7, 10, 30, 31] and further reference are therein. Many experiments for sediment transport have subsequently been conducted during the past years on various bed forms. The one-dimensional natured experiments include the small-scale dam-break problems were detailed in [11], and the stream over a dyke was also studied in the Delft hydraulics laboratory [7]. There are also many two-dimensional experimental studies including a partial dam-break reported in [36], and the groin experiment conducted in [1]. These experimental investigations have been very useful for quantitative and qualitative understandings of hydrodynamics as well as morphodynamics at a laboratory scale. However, one aspect that is rarely measured, is the vertical distribution of sediments within the fluid. This is mainly due to its complex nature and the difficulties in sampling of developing flows without altering the movement of sediments or the speed of fluids. In the present work, these problems are overcame by utilizing a simple small scale one-dimensional flow and image processing along with color content to measure both sediment transport and water flow. This method still presents a number of difficulties such as, parallax error, effects of lighting and water surface effects. These drawbacks are eliminated in part by using the color content, disregarding the background among others, and considering the images gathered in both the RGB in HSI color domains to give the best results. It should be stressed that vertical distribution of sediments is very important for a full understanding of sediment transport in water flows. The techniques implemented in our study would provide a new efficient and low cost approach for gathering sediment distribution data in dam-break problems.

There exists many models for suspended sediments in water flows with different empirical formulae for each type of load under study. One of the earliest and the most recognized relation was formed from the work conducted by Shields in [34]. Indeed, Shields has created the foundation for a lot of the work conducted nowadays, but it has a series of limits due to the ranges over which the data was generated (such as grain size and Reynolds numbers). However, the line between the initiation of motion and the entrainment of particles into the flow was, as Sheilds explained, difficult to assess. Extensive work has been carried out to improve this analysis and develop consistent relations for suspended sediments, see for example [8, 29, 25]. Most natural bodies of water in which sediment transport is a major feature, such as rivers and coastal waters, may be approximated by shallow water flows obtained by depth-averaging the complex free-surface flows, see [13, 26, 27, 41, 40, 14, 23] among others. For the modeling of morphodynamics in shallow water flows, the three most popular models are the Grass model [19], the Meyer-Peter & Muller model [24] and the Van-Rijn model [29]. A large amount of work has also been performed on the effects of water flows on sediment beds, see for example [32,

39, 38, 5]. The predominant approach to sediment transport problems is to rely on empirical data sets, or semi-empirical relations derived from these data sets, see [33] among others. The scale of these approaches can vary widely, from particulate tracking [15], to whole estuary simulations using sediment balance models [15].

In general, the incompressible Navier-Stokes equations have been widely used as the basis for a large number of models and solutions in this field. However, the use of a fully three-dimensional approach for these flows in sediment transport simulations presents challenging formulations and it is computationally expensive. Therefore, modelling simplifications are often preferable, see [23] and further references are therein. One notable development in this direction consists of multilayer shallow water models which offer, a more efficient and accurate flow description. Both miscible [3, 2, 18] and immiscible layered models [20] have been considered in the literature. The advantage of both models is that they avoid the computationally expensive solutions of three-dimensional flows while returning stratified velocities (in two space dimensions). The shallow water equations, can be derived from the non-stationary three-dimensional Navier-Stokes equations, see for example [3, 18]. In the presented work, a novel miscible multilayer model is developed, this model includes movable beds and transport of sediments. The formulation of the model consists of a set of multilayer shallow water equations coupled to a set of transport equations for the suspended sediments in each layer, and a set of semi-empirical equations for erosion and deposition are used. Intra-layer mass movement is captured through mass exchange terms in both the water flow and the sediment concentrations. Thus, each layer is able to have a varying sediment concentration and flow velocities to it neighboring layers. Other models in [21] have similar resolution for the vertical concentration, but the proposed multilayer model does not require computationally demanding vertical discretizations. Recently, a similar work has been extended to account for turbulent kinetic energy in [43]. The focus in the present work is on developing a framework within which empirical or semi-empirical relations as those reported in [43] can be easily incorporated into the numerical model as required. For the entrained sediments we use the equations proposed in [9] but the presented formulation allows for other erosion and deposition equations to be easily incorporated such as those reported in [16, 22, 19, 24].

Solving the multilayer shallow water equations numerically is a complex problem owing to their nonlinear nature as well as the source terms and the free-surface aspects, compare [3, 2] among others. The inclusion of bed-load and suspended sediment equations in the multilayer model creates even more complexities to a numerical solver for this fully coupled system. The problem arises from the coupling terms in these models that encompass derivatives of the unknown physical variables, that the result in the system becoming non-conservative and even non-hyperbolic. As a result, numerical methods originally developed for multilayer shallow water equations over fixed beds will encounter instabilities if applied individually to each layer. In the current study, we implement the Finite Volume Characteristics (FVC) method developed in [6] for solving single-layer shallow water equations. As well as being second-order accurate, the FVC method circumvents the solution of Riemann problems as it is a predictor-corrector type method. In the predictor stage, the method of

characteristics is used to reconstruct the numerical fluxes while the corrector stage recovers to the conservation equations using the finite volume discretization. As shown in [2, 31], the considered FVC method has been used to solve a class of multilayer shallow water equations. As shown in these studies, the FVC method is simple, conservative, non-oscillatory, and a practical solver for multilayer shallow water flows over movable beds. In the present work, further improvements to the FVC method have implemented including: (i) a third-order Runge-Kutta scheme is applied to the time integration; (ii) a second-order splitting operation is used for the solution of the source terms, and; (iii) a cubic Spline interpolation is utilized in the predictor stage. We present numerical results in order to verify the multilayer shallow water flows over erodible beds. Finally, we demonstrate the ability of the proposed model for calculating lateral and vertical distributions of velocities for a multilayer dam-break flow over erodible bed.

This paper is organized as follows: In Section 2 we present a full description of the experimental set-up used and discuss the difficulties to overcome and potential sources of errors. In Section 3 we introduce the mathematical equations governing multilayer shallow water flows over a sedimentary topography. In Section 4, the numerical method for solving the governing equations is formulated. Included in this section is the reconstruction of numerical fluxes by applying the method of characteristics and the discretization of source terms in the model. Experimental and numerical results are presented in Section 5. Finally, Section 6 contains some concluding remarks.

2 Experimental set-up for attaining vertical distribution of sediments in dam-break flows

This section overviews the experimental methods used to calculate the vertical distribution of sediments in a one-dimensional dam-break flow. It focuses on both the physical techniques that are involved in creating the dam-break, as well as overviewing the digital processing techniques required to extract the measured data. It further describes the design and tuning process that was used to create accurate and repeatable results. Commercial image processing tools were used as they provide a basic toolbox that could be quickly adapted for the purposes of this study. The sizing of the entire experiment was of great concern and were dictated by the photographic equipment available and the sediment sizes. There have been a number of small scale one-dimensional dam-break problems which have already been investigated at various lengths from, the 1.2 m Taipei experiment in [11] to the 6 m long Hanyang University experiments in [28]. With the aim to achieve a 0.5 mm to pixel precision, a camera with $1080p$ resolution and $100fps$ is used in our experiment. For the presented results, the bed is formed of a well-graded soil in the range of 1 mm to 0.16 mm and with an averaged particle size $d = 0.25\ mm$. Consequently, the domain was set to a length of 900 mm and, to enable workability and minimal edge effects, the domain width was fixed at 75 mm. The dam-break height was initially

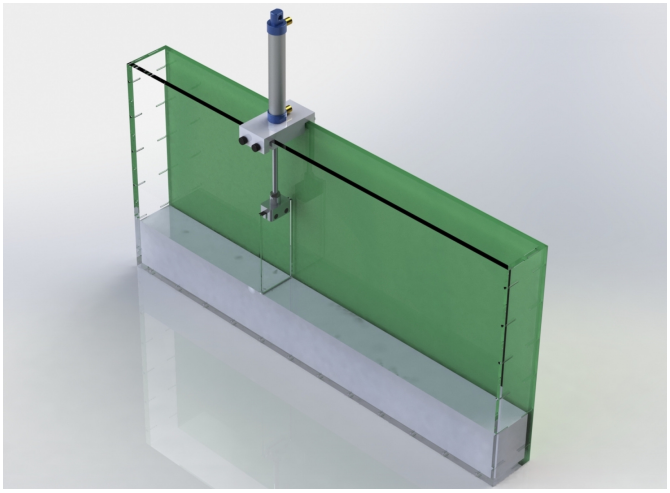

Fig. 1 Design illustration of the experimental rig showing a fixed bed used in the present work.

made at 100 *mm*. and following testing it was increased to 120 *mm* to amplify the erosion observed. Having decided upon the overall dimensions, the mechanism was designed. An electronically controlled pneumatic valve was used to minimize human error and the opening time. The target set was to allow for a dam-break to occur in less than 0.02 *s*. The available line pressure available was 10 *bar* and a small tracking cylinder initially trialled. A range of designs were tested, a directly coupled linear actuator in its simplest configuration was found to be the quickest and most repeatable with an averaged opening time of 0.011 *s*. A bead of sealant was placed in a rebate along the edges of the dam so as to seal the edged but not impair the opening of the dam. The sealant reduced the averaged opening time to 0.018 *s* which was still acceptable. One conclusion that emerged early on, was that even if the bed is compacted it will still would seep. A range of sediments were trialled from ABS spheres at 6 *mm* to fine sand at 0.25 *mm*, nonetheless the seepage beneath the dam undermined to an impractical extent before a differential head of 100 *mm* could be achieved. Consequently, a solid apron behind the dam was implemented as shown in Figure 6.

In order to maximize effects of the high intensity lighting used, transparent ends and a high-sided fixed-end tank were used. This diverged from other open-ended or re-circulating tanks that are more normally used during studies of this type. The dam is positioned at 330 *mm* from the left hand-side which allows 640 *mm* for the dam-break to run over as shown in Figure 6. This maximizes the flow evolution before it reaches the end of the tank, giving an experimental time of 0.42 *s* over a fixed low slip bed and a 0.48 *s* over a high friction sand bed. The high quality consumer grade camera was able to control for photographic concerns like white balance amongst other concerns (these were also checked by eye and able to be modified if required). All other laboratory conditions were maintained throughout

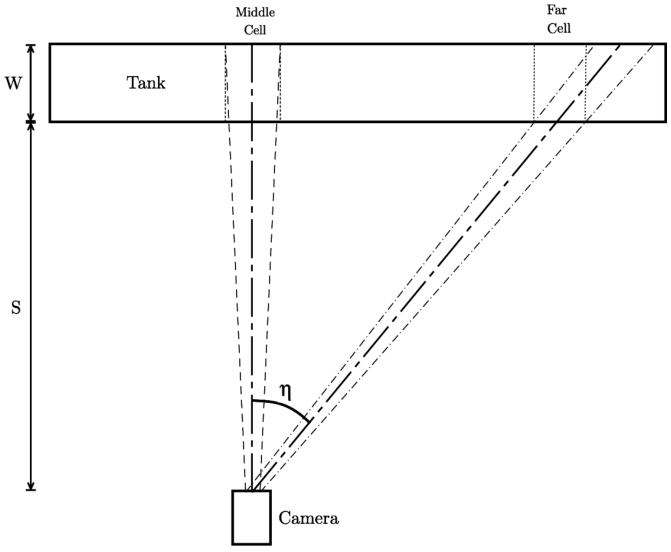

Fig. 2 A sketch detailing the problem of parallax errors related to high-speed camera.

the experiments as far possible. In order to mitigate the errors produced by a single camera recording, a variety of post-processing measures were implemented. The first addressed was parallax error as shown in Figure 2, the greater the orthogonal distance from the camera position the more skewed the image captured would be, which would affect the sediment calculations. Three mitigations were put in place: (i) the camera was centered at 450 *mm* not at the dam-break; (ii) a tele-centric lens was used and a cell neighbor averaging calculation was implemented.

A parallax error also affected the vertical dimension of the images, though to a lesser extent than in the horizontal dimension. The next issue was that the mapping of pixels dominated by the bed into the fluid cells would artificially increase the measured concentration. Balanced against the need to capture the bed-load this became a complex issue. Two steps were used to reduce this error: first, the camera was positioned at the bed height and as erosion in these experiments was minimal this almost eradicated the problem. Second, the bed height was extracted at the light change using the human eye (though in the future it is hoped to use a deep vision approach). This was possible as the increased voids in bed load as compared to a packed bed, created a noticeable light change. Algorithms were initially trialled to discern this but proved to be less accurate and more time consuming than blowing up the image and implementing a dragging point click interpolation method. Thus, the following procedure is developed to correct these raw images and extract the required data:

1. The white balanced was checked against the standard and corrected if necessary;
2. The bed and water surfaces were mapped by a point-click method and parallax errors were computed;

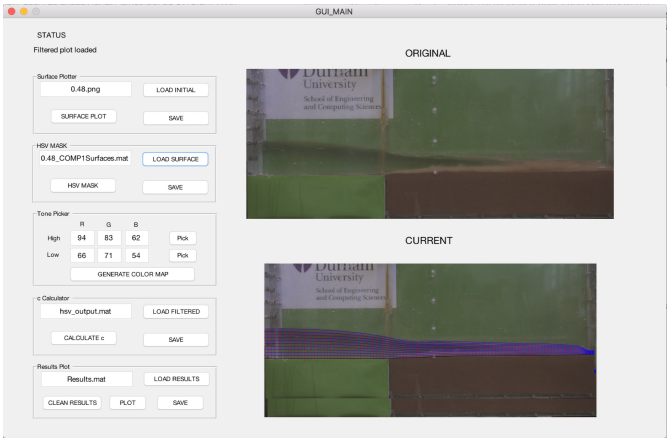

Fig. 3 A screenshot of the automated program used in the current work.

3. Irrelevant background pixels were removed and any remaining hue/lighting errors were corrected by multiple HSI masks;
4. A sediment color chart was created for each experimental run using known high and low areas;
5. The image was then broken down into cells and the depth-averaged concentration by interpolated from the color chart and the cell average;
6. The results were checked against the quantity of erosion in the experiment. This step also allows for an error measure to be made.

It should be stressed that, although this procedure requires some human interaction in step 2, all other steps were automated and incorporated into a graphical user interface (GUI) as shown in Figure 3.

3 Mathematical models for vertical distribution of sediments in dam-break flows

Multilayer flow systems are mainly obtained using a vertical discretization of the three-dimensional Navier-Stokes equations accounting for of shallow water assumptions, compare [2, 3, 4] and further references are therein. In the present study, we consider the one-dimensional version of the model to each of the layers in the fluid and include models for sediment transport accounting for mass exchange between the layers and intra-layer forces between the erodible bed and the water flow. In a multilayer system of a total number of M layers, the shallow water equations for each layer $k = 1,2,\ldots,M$ read as

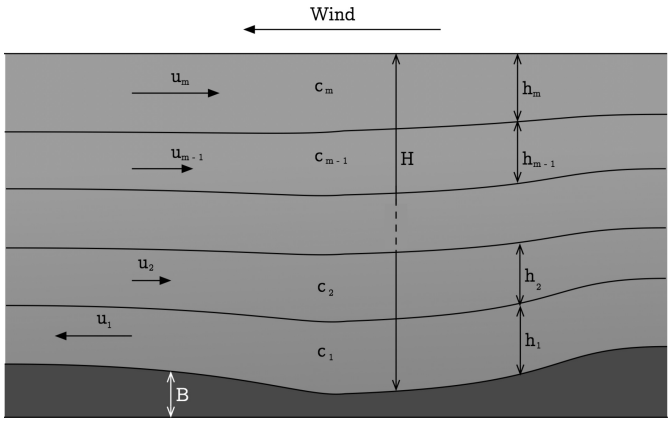

Fig. 4 A simple illustration of multilayer shallow water flows over erodible beds. Each layer k ($k = 1, 2, \ldots, M$) is characterized with a water height h_k, a water velocity u_k, and a sediment concentration c_k. The initial bed is denoted by B.

$$\begin{aligned} \frac{\partial h_k}{\partial t} + \frac{\partial (h_k u_k)}{\partial x} &= G_{k-1/2} - G_{k+1/2}, \\ \frac{\partial (h_k u_k)}{\partial t} + \frac{\partial}{\partial x}\left(h_k u_k^2 + \frac{1}{2} g h_k^2\right) &= -g h_k \frac{\partial B}{\partial x} + F_k, \end{aligned} \tag{1}$$

where u_k is the depth-averaged water velocity of the kth layer, B the bottom topography, g the gravitational acceleration, and h_k the water height of the kth layer defined as

$$h_k = l_k H, \qquad k = 1, \ldots, M, \tag{2}$$

where H is the total water depth and l_k is the proportional height of the layer, see Figure 4 for an illustration. In (1), F_k includes the intra-layer forces defined below and $G_{k\pm1/2}$ are mass exchange terms between the layers including erosion and deposition in the lower layer defined as

$$G_{k-1/2} = \begin{cases} \displaystyle\sum_{\beta=1}^{k} \left(\frac{\partial (h_\beta u_\beta)}{\partial x} - l_\beta \sum_{\gamma=1}^{M} \frac{\partial h_\gamma u_\gamma}{\partial x} \right) + \frac{E_k - D_k}{1-p}, & \text{if} \quad k = 2, \ldots, M, \\ -\dfrac{E_1 - D_1}{1-p}, & \text{if} \quad k = 1, \end{cases}$$

with E_k and D_k represent the entrainment and deposition terms in the upward and downward directions, respectively. Following the same procedure as in[3], we sum the first equation in (1) for all the layers to obtain a single equation for the total water height H as

$$\frac{\partial H}{\partial t} + \sum_{k=1}^{M} \frac{\partial}{\partial x}(h_k u_k) = \frac{E_1 - D_1}{1-p}.$$

In the current study, we also consider bed-load and suspended sediments within the multilayer shallow water system (1). To this end, we define the depth-averaged concentration c_k for the kth layer as

$$c_k = \frac{\rho_k - \rho_w}{\rho_s - \rho_k}, \tag{3}$$

where p is the porosity, ρ_w the water density, ρ_s the sediment density and ρ_k is the density of the water-sediment mixture in the layer k. Hence, the governing equations we consider for modeling multilayer shallow water flows over erodible beds are given as

$$\begin{aligned}
\frac{\partial H}{\partial t} + \sum_{k=1}^{M} \frac{\partial (h_k u_k)}{\partial x} &= \frac{E_1 - D_1}{1-p}, \\
\frac{\partial (h_k u_k)}{\partial t} + \frac{\partial}{\partial x}\left(h_k u_k^2 + \frac{1}{2} g h_k^2\right) &= -g h_k \frac{\partial B}{\partial x} - \frac{(\rho_s - \rho_w)}{2\rho_k} g h_k^2 \frac{\partial c_k}{\partial x} + F_k, \\
\frac{\partial (h_k c_k)}{\partial t} + \frac{\partial (h_k u_k c_k)}{\partial x} &= E_k - D_k - c_{k+1/2} G_{k+1/2} + c_{k-1/2} G_{k-1/2} - \\
&\qquad \epsilon \left(\frac{\partial^2 c_{\Delta+1/2}}{\partial z^2} - \frac{\partial^2 c_{\Delta-1/2}}{\partial z^2} \right), \\
\frac{\partial B}{\partial t} &= -\frac{E_1 - D_1}{1-p},
\end{aligned} \tag{4}$$

where E_1 and D_1 are the erosion and deposition rates on the bottom fluid layer, respectively. In this study, the inter-layer diffusion in the concentration is handled by considering the diffusion potential between two layers $c_{\Delta,k-1/2}$ and $c_{\Delta,k+1/2}$ and a diffusion coefficient ϵ. Note that these terms are included in the model to handle the sediment diffusion. In (4), the external force F_k acting on the kth layer accounting for friction and momentum exchange effects is given by

$$F_k = F_k^{(u)} + F_k^{(b)} + F_k^{(w)} + F_k^{(\mu)}, \tag{5}$$

with $F_k^{(u)}$ is related to the momentum exchange between the layers by

$$F_k^{(u)} = u_{k+1/2} G_{k+1/2} - u_{k-1/2} G_{k-1/2} - \frac{1}{l_k} \frac{(\rho_0 - \rho_k)(E_k - D_k) u_k}{\rho_k (1-p)}.$$

where ρ_0 is the density of the saturated bed related to the porosity as

$$\rho_0 = \rho_w p + \rho_s (1-p),$$

and the intermediate velocity $u_{k+1/2}$ is reconstructed using an upwind method based on the sign of the mass exchange term as

$$u_{k-1/2} = \begin{cases} u_{k-1}, & \text{if} \quad G_{k-1/2} \geq 0, \\ u_k, & \text{otherwise.} \end{cases}$$

The vertical kinematic eddy viscosity term $F_k^{(\mu)}$ in (5) takes into account the friction between neighboring layers as

$$F_k^{(\mu)} = \begin{cases} -2\nu \dfrac{u_{k-1} - u_k}{(l_{k-1} + l_k)H}, & \text{if} \quad k = M, \\ 2\nu \dfrac{u_{k+1} - u_k}{(l_{k+1} + l_k)H} - 2\nu \dfrac{u_{l-1} - u_k}{(l_{k-1} + l_k)H}, & \text{if} \quad k = 2, \ldots, M-1, \\ 2\nu \dfrac{u_{l+1} - u_k}{(l_{k+1} + l_k)H}, & \text{if} \quad k = 1, \end{cases}$$

where ν is the eddy viscosity. The external bed friction term $F_k^{(b)}$ in (5) is given as

$$F_k^{(b)} = \begin{cases} -\dfrac{g n_b^2}{H^{1/3}} u_1 |u_1|, & \text{if} \quad k = 1, \\ 0, & \text{otherwise,} \end{cases} \tag{6}$$

where n_b is the Manning roughness coefficient. The surface wind force $F_k^{(w)}$ in (5) is defined as

$$F_k^{(w)} = \begin{cases} -\dfrac{\sigma^2 \rho_a}{H} w|w|, & \text{if} \quad k = M, \\ 0, & \text{otherwise,} \end{cases} \tag{7}$$

where w is the relative wind velocity at 10 m above the water surface and σ is the wind stress coefficient. Note that for the bottom layer, an equation that relates the effects of an erodible bed is included in the model (1). These equations are presented in a very general form such that appropriate empirical erosion and deposition equations can be substituted with ease. Thus, to determine the entrainment and deposition terms in (1) we assume a non-cohesive sediment and we use the empirical relations reported in [9]

$$D_k = \begin{cases} w_s (1 - C_a)^m C_a, & \text{if} \quad k = 1, \\ 0, & \text{otherwise,} \end{cases} \tag{8}$$

where w_s is the deposition coefficient experimentally measured in [30, 42, 33], d the averaged diameter of the sediment particle, m an exponent indicating the effects of hindered settling due to high sediment concentrations, $C_a = \beta_c c_k$ is the near-bed volumetric sediment concentration. Here, β_c is a coefficient larger than unity used to ensure that the near-bed concentration does not exceed $(1 - p)$ and it is defined

in [10] by

$$\beta_c = \min\left(2, \frac{1-p}{c_k}\right).$$

For the entrainment of the material the following relation is used

$$E_k = \begin{cases} \varphi \dfrac{\theta - \theta_c}{h_1} u_1 d^{-0.2}, & \text{if} \quad \theta \geq \theta_c \quad \text{and} \quad k = 1, \\ 0, & \text{otherwise,} \end{cases} \tag{9}$$

where φ is a coefficient to control the erosion forces, θ_c is a critical value of Shields parameter for the initiation of sediment motion and θ is the Shields coefficient defined by

$$\theta = \frac{u_*^2}{sgd},$$

with $s = \frac{\rho_s}{\rho_w} - 1$ is the submerged specific gravity of sediment and u_* is the friction velocity defined as

$$u_*^2 = \sqrt{\frac{g\, n_b^2}{h^{1/3}}}\, |u_1|\,.$$

Note that the equations used for the entrainment and deposition have been widely used in the literature for the conventional single-layer shallow water flows over erodible beds, see for example [30, 42, 33, 5]. It should also be pointed out that no vertical velocities are calculated in the proposed model, but the vertical sediment diffusion is a major problem for a formulation of this type. In this study, a sediment diffusion coefficient ϵ is introduced in the multilayer model (4).

For ease of presentation, we re-arrange the governing equations (4) into a compact vector form as

$$\frac{\partial \mathbf{W}}{\partial t} + \frac{\partial \mathbf{F}(\mathbf{W})}{\partial x} = \mathbf{Q}(\mathbf{W}) + \mathbf{R}(\mathbf{W}), \tag{10}$$

where $\mathbf{W}$ is the vector of conserved variables, $\mathbf{F}(\mathbf{W})$ is the vector of flux functions, $\mathbf{Q}(\mathbf{W})$ and $\mathbf{R}(\mathbf{W})$ are the vectors of source terms defined by

$$\mathbf{F}(\mathbf{W}) = \begin{pmatrix} \sum_{\alpha=1}^{k} l_\alpha H u_\alpha \\ H u_1^2 + \frac{1}{2} g H^2 \\ H u_1 c_1 \\ H u_2^2 + \frac{1}{2} g H^2 \\ H u_2 c_2 \\ \vdots \\ H u_k^2 + \frac{1}{2} g H^2 \\ H u_k^2 + \frac{1}{2} g H^2 \\ H u_k c_k \\ 0 \end{pmatrix}, \qquad \mathbf{Q}(\mathbf{W}) = \begin{pmatrix} 0 \\ -gH\frac{\partial B}{\partial x} - \frac{(\rho_s - \rho_w)}{2\rho_1} g l_1 H^2 \frac{\partial c_1}{\partial x} \\ 0 \\ -gH\frac{\partial B}{\partial x} - \frac{(\rho_s - \rho_w)}{2\rho_2} g l_2 H^2 \frac{\partial c_2}{\partial x} \\ 0 \\ \vdots \\ -gH\frac{\partial B}{\partial x} - \frac{(\rho_s - \rho_w)}{2\rho_k} g l_M H^2 \frac{\partial c_k}{\partial x} \\ 0 \\ 0 \end{pmatrix},$$

$$\mathbf{W} = \begin{pmatrix} H \\ H u_1 \\ H c_1 \\ H u_2 \\ H c_2 \\ \vdots \\ H u_k \\ H u_k \\ H c_k \\ B \end{pmatrix}, \qquad \mathbf{R}(\mathrm{W}) = \begin{pmatrix} \frac{E_1 - D_1}{1-p} \\ -\frac{1}{l_1}\left(F_1^{(u)} + F_1^{(b)} + F_1^{(\mu)}\right) \\ E_1 - D_1 - G_{3/2} c_{3/2} - \epsilon \frac{\partial^2 c_{\Delta,3/2}}{\partial z^2} \\ -\frac{1}{l_2}\left(F_2^{(u)} + F_2^{(\mu)}\right) \\ G_{5/2} c_{5/2} - G_{3/2} c_{3/2} + \epsilon \frac{\partial^2 c_{\Delta,3/2}}{\partial z^2} - \epsilon \frac{\partial^2 c_{\Delta,5/2}}{\partial z^2} \\ \vdots \\ -\frac{1}{l_k}\left(F_k^{(u)} + F_k^{(w)} + F_k^{(\mu)}\right) \\ -G_{M-1/2} c_{M-1/2} + \epsilon \frac{\partial^2 c_{\Delta,M-1/2}}{\partial z^2} \\ -\frac{E_1 - D_1}{1-p} \end{pmatrix}.$$

It should be stressed that the source term $\mathbf{Q}$ contains the first-order differential terms with respect to the coordinate x, while the remaining forces are included in the source term $\mathbf{R}$. This structure is advantageous as it allows for a time splitting operator in (10), for which the source terms $\mathbf{Q}$ and $\mathbf{R}$ are treated separately in different stages of the splitting.

4 Numerical methods for vertical distribution of sediments in dam-break flows

To integrate the system (4), time is divided into subintervals $[t_n, t_{n+1}]$ with length $\Delta t = t_{n+1} - t_n$ and the notation $\mathbf{W}^n$ is used to denote the value of a generic function $\mathbf{W}$ at time t_n. Here, a second-order splitting procedure, like[37] is used, and carried out in three stages as:

Stage 1: Solve for $\mathbf{W}^*$

$$\begin{aligned} \frac{\partial \mathbf{W}^*}{\partial t} &= \mathbf{R}(\mathbf{W}^*), \qquad t \in [t_n, t_{n+1/2}], \\ \mathbf{W}^*(t_n) &= \mathbf{W}(t_n). \end{aligned} \tag{11}$$

Stage 2: Solve for $\mathbf{W}^{**}$

$$\begin{aligned} \frac{\partial \mathbf{W}^{**}}{\partial t} + \frac{\partial \mathbf{F}(\mathbf{W}^{**})}{\partial x} &= \mathbf{Q}(\mathbf{W}^{**}), \qquad t \in [t_n, t_{n+1}], \\ \mathbf{W}^{**}(t_n) &= \mathbf{W}^*(t_{n+1/2}). \end{aligned} \tag{12}$$

Stage 3: Solve for $\mathbf{W}^{***}$

$$\begin{aligned} \frac{\partial \mathbf{W}^{***}}{\partial t} &= \mathbf{R}(\mathbf{W}^{***}), \qquad t \in [t_{n+1/2}, t_{n+1}], \\ \mathbf{W}^{***}(t_{n+1/2}) &= \mathbf{W}^{**}(t_{n+1}). \end{aligned} \tag{13}$$

To complete the time integration, the explicit third-order Runge-Kutta method [35] is used for each stage in (11)-(13). For instance, to advance the solution of (11) from time t_n to time t_{n+1} the following is used

$$\begin{aligned} \mathcal{W}^{(1)} &= \mathbf{W}^n + \Delta t \mathbf{R}(\mathbf{W}^n), \\ \mathcal{W}^{(2)} &= \frac{3}{4}\mathbf{W}^n + \frac{1}{4}\mathcal{W}^{(1)} + \frac{1}{4}\Delta t \mathbf{R}(\mathcal{W}^{(1)}), \\ \mathbf{W}^{n+1} &= \frac{1}{3}\mathbf{W}^n + \frac{2}{3}\mathcal{W}^{(2)} + \frac{2}{3}\Delta t \mathbf{R}(\mathcal{W}^{(2)}). \end{aligned} \tag{14}$$

The asterisk is dropped off of the variables for ease in the notation. Note that the Runge-Kutta method (14) is total variation diminishing (TVD), third-order accurate in time, and stable under the usual Courant-Friedrichs-Lewy (CFL) condition involving eigenvalues of the system under study. It should also be noted that explicit expressions of the eigenvalues for the system (10) are not trivial to find and as for multilayer shallow water equation over fixed beds there may exist situations for which eigenvalues become complex. In these cases, the multilayer system (10) is not hyperbolic and yields to the so-called Miles-Howard instability at the water interfaces [12]. As a consequence, most finite volume methods which are based on Riemann solvers would fail to resolve the system (10) for the multilayer shal-

low water equations over erodible beds. In the present study, we consider the Finite Volume Characteristics (FVC) method introduced in [6] and used in [2] for the numerical solution of multilayer shallow water flows over fixed beds. In this section, we briefly describe the FVC formulation for the system (10) and further details can be found in [6, 2]. Note that the FVC method does not require the calculation of the eigenvalues for the multilayer system (4). However, the selection of time steps is carried out using the eigenvalues associated with the single-layer counterpart of the system (4) which are defined in [5] as

$$\begin{aligned} &\lambda_1 = 0, \\ &\lambda_{2,k} = u_k, \quad \lambda_{3,k} = u_k - \sqrt{g h_k}, \quad \lambda_{4,k} = u_k + \sqrt{g h_k}, \qquad k = 1,2\ldots,M. \end{aligned} \tag{15}$$

Note that the eigenvalues (15) are for the single-layer sediment transport system associated with (4) using the water heights h_k and not the total height H. This results in a system of $(3M + 1)$ equations for which each uncoupled layer, its associated four eigenvalues are given by (15). It should also be stressed that similar approach has been considered in [2] for multilayer shallow water flows over fixed beds for which eigenvalues of it single-layer counterpart have been used in the simulations. In the current study, the courant number is set to $Cr = 0.85$ in all the computations and the time stepsize Δt is adjusted at each step according to the CFL condition

$$\Delta t = Cr \frac{\Delta x}{\max\limits_{k=1,2,\ldots,M} \left(|\lambda_1|, |\lambda_{2,k}|, |\lambda_{3,k}|, |\lambda_{4,k}|\right)},$$

where Δx is the spatial discretization step, λ_1, $\lambda_{2,k}$, $\lambda_{3,k}$ and $\lambda_{4,k}$ are the approximated eigenvalues in (15).

4.1 Spatial discretization

The spatial domain is discretized into control volumes $[x_{i-1/2}, x_{i+1/2}]$ centered at x_i with a step size Δx. For the space discretization of the equations (12), the following notations are used

$$\mathbf{W}_{i\pm\frac{1}{2}}(t) = \mathbf{W}(t, x_{i\pm\frac{1}{2}}), \qquad \mathbf{W}_i(t) = \frac{1}{\Delta x} \int_{x_{i-\frac{1}{2}}}^{x_{i+\frac{1}{2}}} \mathbf{W}(t,x)dx,$$

to denote the point-values and the approximate cell-average of the variable $\mathbf{W}$ at the gridpoint $(t, x_{i\pm\frac{1}{2}})$ and (t, x_i), respectively. Integrating the equation (12) with respect to space over the control volume, the following semi-discrete equations are obtained

$$\frac{d\mathbf{W}_i}{dt} + \frac{\mathbf{F}_{i+1/2} - \mathbf{F}_{i-1/2}}{\Delta x} = \mathbf{Q}_i, \tag{16}$$

where $\mathbf{F}_{i\pm1/2} = \mathbf{F}(\mathbf{W}_{i\pm1/2})$ are the numerical fluxes at the cell interfaces $x = x_{i\pm1/2}$. In equation (12), $\mathbf{Q}_i$ is a consistent discretization of the source term $\mathbf{Q}$ in (12). In order to reconstruct the numerical fluxes $\mathcal{F}^n_{i\mp1/2}$, the Method of Characteristics (MoC) is applied to the advective version of the system (12). Without accounting for the source term $\mathbf{R}(\mathbf{W})$ we reformulate the equations in (12) into the following advective form

$$\begin{aligned}
&\frac{\partial H}{\partial t} + \Big(\sum_{j=1}^{M} l_j u_j\Big)\frac{\partial H}{\partial x} = -\sum_{j=1}^{M} l_j H \frac{\partial u_j}{\partial x},\\
&\frac{\partial Q_k}{\partial t} + u_k \frac{\partial Q_k}{\partial x} = -Q_k \frac{\partial u_k}{\partial x} - gH\frac{\partial (H+B)}{\partial x} - \frac{(\rho_s-\rho_w)}{2\rho_k} g l_k H^2 \frac{\partial c_k}{\partial x},\\
&\frac{\partial P_k}{\partial t} + u_k \frac{\partial P_k}{\partial x} = -P_k \frac{\partial u_k}{\partial x},
\end{aligned}$$

where the discharge $Q_k = Hu_k$ and the sediment remittance $P_k = Hc_k$. The above system can also be rearranged in a compact vector form as

$$\frac{D_k U_k}{Dt} = S_k\left(\mathbf{U}\right), \qquad k = 0,1,2,\ldots,2M, \tag{17}$$

with $\frac{D_k}{Dt}$ is the total derivative defined by

$$\frac{D_k}{Dt} = \frac{\partial}{\partial t} + \mathcal{U}_k \frac{\partial}{\partial x}, \qquad k = 0,1,2,\ldots,2M, \tag{18}$$

where $\mathbf{U} = (U_0, U_1, \ldots, U_{2M})^T$, $\mathbf{S}\left(\mathbf{U}\right) = (S_0, S_1, \ldots, S_{2M})^T$ with

$$\mathbf{U} = \begin{pmatrix} H \\ Q_1 \\ P_1 \\ \vdots \\ Q_M \\ P_M \end{pmatrix}, \quad \mathbf{S}(\mathbf{U}) = \begin{pmatrix} -\sum_{j=1}^{M} l_j H \frac{\partial u_j}{\partial x} \\ -Q_1 \frac{\partial u_1}{\partial x} - gH\frac{\partial\left(H+B\right)}{\partial x} - \frac{(\rho_s-\rho_w)}{2\rho_1} g l_1 H^2 \frac{\partial c_1}{\partial x} \\ -P_1 \frac{\partial u_1}{\partial x} \\ \vdots \\ -Hu_M \frac{\partial u_M}{\partial x} - gH\frac{\partial\left(H+B\right)}{\partial x} - \frac{(\rho_s-\rho_w)}{2\rho_M} g l_M H^2 \frac{\partial c_M}{\partial x} \\ -P_M \frac{\partial u_M}{\partial x} \end{pmatrix},$$

and the advection velocity $\mathcal{U}_k$ is defined as

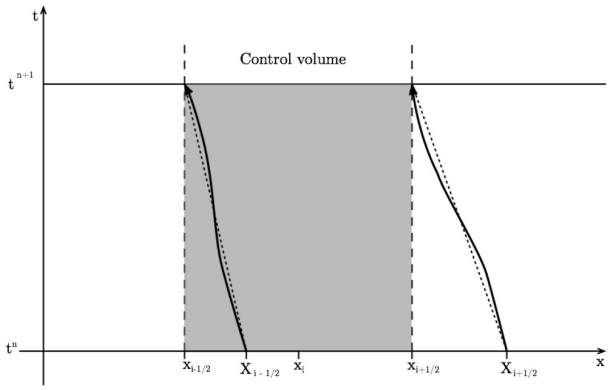

Fig. 5 A schematic diagram showing a control volume and the main quantities used in the calculation of the departure points $X_{i+1/2}(\tau)$ that will reach $x_{i+1/2}$ at time t_{n+1}. The exact trajectory is represented by a solid line and the approximate trajectory with a dashed line.

$$\mathcal{U}_k = \begin{cases} \displaystyle\sum_{j=1}^{M} l_j u_j, \text{ if} & k = 0, \\ u_{\frac{k+1}{2}}, \text{ if} & k = 1,3,5,\ldots, \\ u_{\frac{k}{2}}, \text{ if} & k = 2,4,6,\ldots. \end{cases} \tag{19}$$

Note that we used $k = 0$ in the above equations to only formulate the compact advective form (17) for all the equations and it does not refer to any layer in the system. The principal idea of the FVC method is to use the method of characteristics to approximate the numerical fluxes in (16). Hence, the characteristic curves associated with the system (17) are solutions of the initial-value problems

$$\begin{aligned} &\frac{dX_{k,i+1/2}(\tau)}{d\tau} = \mathcal{U}_{k,i+1/2}\Big(\tau, X_{k,i+1/2}(\tau)\Big), \quad \tau \in [t_n, t_{n+1}], \\ &X_{k,i+1/2}(t_n) = x_{i+1/2}, \qquad k = 0,1,\ldots,2M. \end{aligned} \tag{20}$$

where $X_{k,i+1/2}(\tau)$ is the departure point defined at time τ of a particle that will reach $x_{i+1/2}$ at time t_{n+1}. It should be noted that the FVC method does not follow the flow particles forward in time, as a Lagrangian method does, instead it traces backwards the position at time t_n of particles that will reach the points of a fixed mesh at time t_{n+1}, see Figure 5 for an illustration. Therefore, the FVC method avoids the grid distortion difficulties that the conventional Lagrangian schemes have.

Accurate approximation of the characteristic curves $X_{k,i+1/2}(t_n)$ is crucial to the overall accuracy of the FVC method. Some authors approximate the solutions

of (20) using a second-order explicit Runge-Kutta scheme, which is not accurate enough to maintain a particle on its curved trajectory, see for instance [17]. In [6, 2], a second-order extrapolation based on the mid-point rule is used to approximate the solution of (20), but this method involves an iterative procedure which may become computationally demanding. In the present study, we consider the third-order explicit Runge-Kutta method (14). Thus, the procedure to approximate the solution of the differential equations (20) can be achieved by

$$\begin{aligned} \mathcal{X}^{(1)}_{k,i+1/2} &= \mathbf{x}_{k,i+1/2} - \Delta t \mathcal{U}^{n}_{k,i+1/2}, \\ \mathcal{X}^{(2)}_{k,i+1/2} &= \frac{3}{4} x_{k,i+1/2} + \frac{1}{4}\mathcal{X}^{(1)}_{k,i+1/2} - \frac{1}{4}\Delta t \mathcal{U}^{n}_{k,i+1/2}, \\ X_{k,i+1/2}(t_n) &= \frac{1}{3} x_{k,i+1/2} + \frac{2}{3}\mathcal{X}^{(2)}_{k,i+1/2} - \frac{2}{3}\Delta t \mathcal{U}^{n}_{k,i+1/2}. \end{aligned} \tag{21}$$

It should be stressed that since the departure points $X_{k,i+1/2}(t_n)$ and the stages $\mathcal{X}^{(1)}_{k,i+1/2}$ and $\mathcal{X}^{(2)}_{k,i+1/2}$ would not necessarily lie on a mesh point in the computational domain, the solution at the departure points must be obtained by interpolation from known values at the gridpoints of the element where the points $X_{k,i+1/2}(t_n)$ and the stages $\mathcal{X}^{(1)}_{k,i+1/2}$ and $\mathcal{X}^{(2)}_{k,i+1/2}$ are localized. In the current work, we use the cubic Spline interpolation to approximate the solutions at the characteristics points. Other high-order interpolation procedures can also be applied.

Once the characteristics curves $X_{k,i+1/2}(t_n)$ in (20) are calculated, a solution at the cell interface $x_{i+1/2}$ is approximated as

$$U^{n+1}_{k,i+1/2} := U_k\left(t_{n+1}, x_{i+1/2}\right) = \widetilde{U}_k\left(t_n, X_{k,i+1/2}(t_n)\right), \tag{22}$$

where $\widetilde{U}_k\left(t_n, X_{k,i+1/2}(t_n)\right)$ is the solution at the departure point $X_{k,i+1/2}(t_n)$ approximated by the cubic interpolation using the gridpoints of the control volume where it belongs *i.e.*

$$\widetilde{U}_k\left(t_n, X_{k,i+1/2}(t_n)\right) = \mathcal{P}\Big(U_k\left(t_n, X_{k,i+1/2}(t_n)\right)\Big), \tag{23}$$

where $\mathcal{P}$ is the cubic Spline interpolating operator. Notice that authors in [6, 2] used the Lagrange interpolation polynomials in (23). In what follows we use the first-order Euler scheme to illustrate the formulation of the FVC method but in all our simulations the third-order Runge-Kutta scheme (14) is used. Thus, applied to the equations (17), the characteristic solutions are computed in the predictor stage of the FVC method as

$$
\begin{aligned}
H^{n+1}_{i+1/2} &= \widetilde{H}^{n}_{i+1/2} - \frac{\Delta t}{\Delta x}\widetilde{H}^{n}_{i+1/2}\sum_{k=1}^{M} l_k\left(u^{n}_{k,i+1} - u^{n}_{k,i}\right),\\
Q^{n+1}_{k,i+1/2} &= \widetilde{Q}^{n}_{k,i+1/2} - \frac{\Delta t}{\Delta x}\Bigg(\widetilde{Q}^{n}_{k,i+1/2}\left(u^{n}_{k,i+1} - u^{n}_{k,i}\right) +\\
&\qquad g\widetilde{H}^{n}_{i+1/2}\Big(\left(H^{n}_{i+1} + B^{n}_{i+1}\right) - \left(H^{n}_{i} + B^{n}_{i}\right)\Big) +\\
&\qquad \frac{(\rho_s - \rho_w)}{2\widetilde{\rho}^{n}_{k,i+1/2}} g l_k\left(\widetilde{H}^{n}_{i+1/2}\right)^2\left(c^{n+1/2}_{i+1} - c^{n+1/2}_{i}\right)\Bigg),\\
P^{n+1}_{k,i+1/2} &= \widetilde{P}^{n}_{k,i+1/2} - \frac{\Delta t}{\Delta x}\widetilde{P}^{n}_{k,i+1/2}\left(u^{n}_{k,i+1} - u^{n}_{k,i}\right),
\end{aligned}
\tag{24}
$$

where $\widetilde{H}^{n}_{i+1/2} = H\left(t_n, X_{0,i+1/2}(t_n)\right)$, $\widetilde{Q}^{n}_{k,i+1/2} = Q_k\left(t_n, X_{k,i+1/2}(t_n)\right)$ and $\widetilde{P}^{n}_{k,i+1/2} = P_k\left(t_n, X_{k,i+1/2}(t_n)\right)$ are the solutions at the departure points $X_{k,i+1/2}(t_n)$ computed using the cubic Spline interpolation. To calculate the numerical fluxes $\mathbf{F}_{i\pm1/2} = \mathbf{F}\left(\mathbf{W}_{i\pm1/2}\right)$, the intermediate states $\mathbf{W}_{i\pm1/2}$ are updated using the characteristic solutions $\mathbf{U}_{i\pm1/2}$ in the predictor stage (24). Thus, using the first-order Euler scheme for illustration only, the solution in the FVC method (16) is obtained using the following corrector stage

$$
\begin{aligned}
H^{n+1} &= H^{n} - \frac{\Delta t}{\Delta x}\sum_{k=1}^{M}\left((l_k H u_k)^{n}_{i+1/2} - (l_k H u_k)^{n}_{i-1/2}\right),\\
Q^{n+1}_{k,i} &= Q^{n}_{k,i} - \frac{\Delta t}{\Delta x}\left(\left(H u_k^2 + \frac{1}{2}gH^2\right)^{n}_{i+1/2} - \left(H u_k^2 + \frac{1}{2}gH^2\right)^{n}_{i-1/2}\right) -\\
&\qquad \frac{\Delta t}{\Delta x} g\left(\widehat{H}^{n}_{i}\left(B^{n}_{i+1} - B^{n}_{i-1}\right) - \frac{(\rho_s - \rho_w)}{2\widehat{\rho}^{n}_{k,i}} l_k\left(\widehat{H}^{n}_{i}\right)^2\left(c^{n}_{k,i+1} - c^{n}_{k,i-1}\right)\right),\\
P^{n+1}_{k,i} &= P^{n}_{k,i} - \frac{\Delta t}{\Delta x}\left((H u_k c_k)^{n}_{i+1/2} - (H u_k c_k)^{n}_{i-1/2}\right).
\end{aligned}
\tag{25}
$$

For the reconstruction of the terms $\widehat{H}^{n}_{i}$ and $\widehat{\rho}^{n}_{k,i}$, we use the same concept as in [6, 2] to guarantee that the discretization of the flux gradients and source terms in (16) are well balanced. Hence,

$$
\widehat{H}^{n}_{i} = \frac{1}{4}\left(H^{n}_{i+1} + 2H^{n}_{i} + H^{n}_{i-1}\right), \qquad \widehat{\rho}^{n}_{k,i} = \frac{1}{4}\left(\rho^{n}_{k,i+1} + 2\rho^{n}_{k,i} + \rho^{n}_{k,i-1}\right). \tag{26}
$$

Note that the discretization of equations (11) and (13) is straightforward and it is omitted here. It should also be mentioned that the considered FVC method is fully conservative by construction and the non-conservative system (17) is used only to compute the intermediate states for the numerical fluxes in (16).

Table 1 Sediment parameters for the bed type used in our simulations for the erosion and deposition formulae.

d	p	φ	θ_c	w_s	n_b	ε	ρ_s
0.0625 mm	0.5	0.0004	0.0145	0.0002	0.011	0.005	1420 kg/m^3

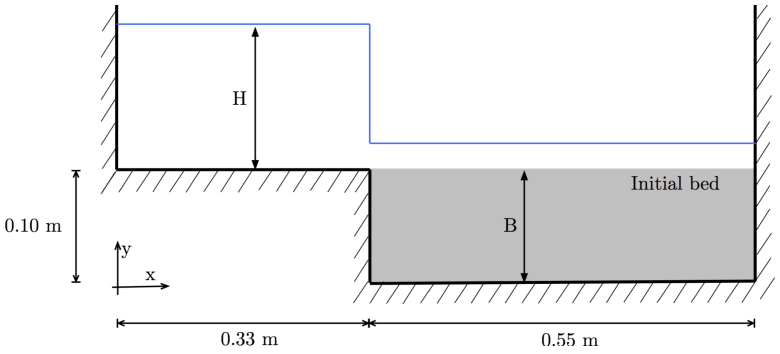

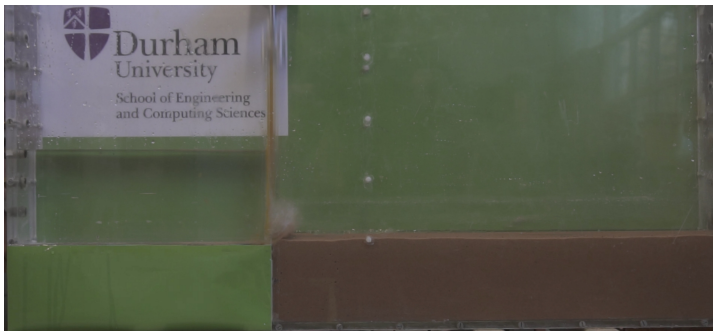

Fig. 6 Configuration of the scour after an apron domain (top) and a photo of the experimental setup (bottom) used in the current study.

5 Experimental and numerical results

The aim of this section is to present both the collected data from the experimental study and compare them to the numerical results obtained using the multilayer shallow water model. This should demonstrate that the measurements are reasonable and validate the computed results. To this end the numerical model is first compared with a three-dimensional Navier-Stokes solver using icoFOAM algorithm on the OpenFOAM software for a dam-break problem over a fixed bed. Then, the experimental data is presented and compared to those results obtained using the FVC method solving the multilayer shallow water equations. We present computational results using the sediment characteristics listed in Table 1. These sediment parameters have been recommended in many experimental studies on sediment transport

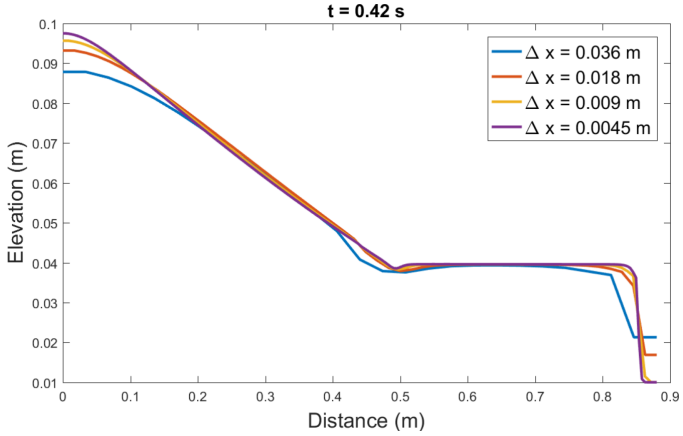

Fig. 7 Numerical results obtained for the water depth using the FVC method on four different meshes for the dam-break problem over a fixed bed.

applications, see for instance [30, 42, 33]. The configuration of the domain along with the experimental setup are illustrated in Figure 6. The experimental work was carried out at the hydraulics laboratory at University of Durham. In our simulations, the water density $\rho_w = 1000\ kg/m^3$, the gravity acceleration $g = 9.81\ m/s^2$ and the number of layers in the multilayer shallow water model is fixed to 10 for all examples in this section.

First we examine the mesh convergence in the proposed FVC method for solving dam-break problems. To this end, we consider the case of dam-break problem over a fixed bed. Hence, $B = 0$ and initially,

$$H(0,x,y) = \begin{cases} 0.10\ m, & \text{if} \quad x \leq 0.33\ m, \\ \\ 0.016\ m, & \text{if} \quad x > 0.33\ m, \end{cases} \qquad u(0,x,y) = 0\ m/s.$$

We consider four meshes with $\Delta x = 0.036\ m$, 0.018 , $0.009\ m$ and $0.0045\ m$ using 10 layers in the multilayer model. The obtained results for the water depth at time $t = 0.42\ s$ are presented in Figure 7. As can be seen for the last two meshes with $\Delta x = 0.009\ m$ and $\Delta x = 0.0045\ m$, the differences in the results obtained for the water depth in Figure 7 are very small. It is easy to see that solutions obtained using $\Delta x = 0.036\ m$ are far from those obtained by the other meshes. Increasing the density of control volumes, the results for the $\Delta x = 0.009\ m$ and $\Delta x = 0.0045\ m$ are roughly similar. Results obtained for the water velocity and not reported here for brevity, show the same trends. This ensures grid convergence of the numerical results. Hence, the mesh with $\Delta x = 0.009\ m$ is used in all our next computations. The reasons for choosing this mesh structure lie essentially on the computational cost required for each mesh configuration and also on the numerical resolution obtained.

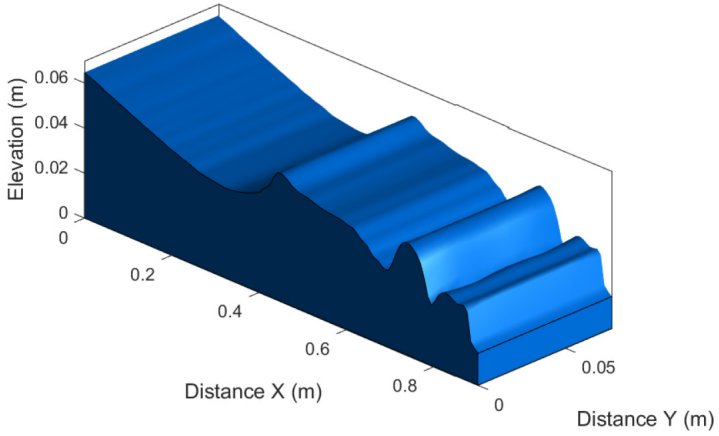

Fig. 8 Three-dimensional results obtained using OpenFOAM simulation for the dam-break problem over a fixed bed at time $t = 0.42\ s$.

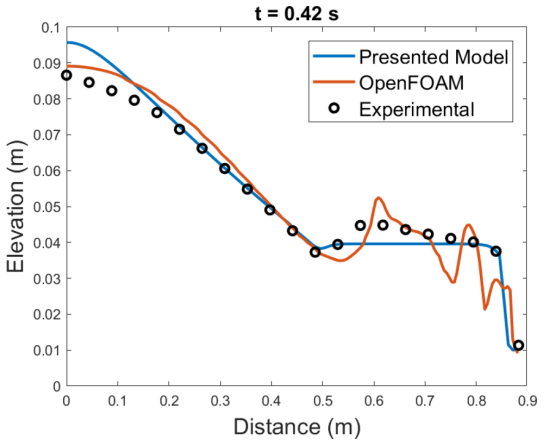

Fig. 9 Comparison between three-dimensional results obtained using OpenFOAM simulation, the proposed multilayer model and the experimental results for the dam-break problem over a fixed bed at time $t = 0.42\ s$.

Our next concern is to validate our results to those obtained using the three-dimensional Navier-Stokes equations. The objective is to discern the ability of the presented model to capture sediment transport in both the horizontal and vertical dimensions. Unfortunately, for this field of research the sedFOAM program, one of the most highly advanced sediment tools in OpenFOAM, it is not able to simulate the dam-break problem presented in this study. Thus, prior ot the addition of sediment to the domain, the dam-break over a fixed bed is considered and the IcoFOAM solver is implemented. In Figure 8 we present the water free-surface obtained at time $t = 0.42\ s$ for the three-dimensional simulations. Here, a mesh with 7569 el-

ements and 4543 nodes is used in the three-dimensional computations along with a fixed time step $\Delta t = 0.01$. A comparison between the cross-section of the IcoFOAM results at $y = 0.05$ and those obtained using the FVC method for 10-layer model is depicted in Figure 9. The experimental results obtained for this case are also included in this figure. It is clear from these results that the location and the speed of the moving water front obtained using the multilayer model agree well to those computed using the three-dimensional IcoFOAM model. Note that fluctuations with different amplitudes appear in the three-dimensional results which are completely absent in the results obtained using the multilayer model. These fluctuations are mainly cause by the two-phase flow equations and turbulent effects accounted for in the IcoFOAM model and are also in good agreement with the experimental for this class of dam-break flows.

We next consider sediment transport in our experimental setup and compare the measured results to those obtained using the FVC method solving the multilayer shallow water equations. At time $t = 0$,

$$B(0,x,y) = \begin{cases} 0\ m, & \text{if} \quad x \leq 0.33\ m, \\ \\ 0.00475\ m, & \text{if} \quad x > 0.33\ m, \end{cases} \qquad c(0,x,y) = 0,$$

and

$$H(0,x,y) = \begin{cases} 0.12\ m, & \text{if} \quad x \leq 0.33\ m, \\ \\ 0.016\ m, & \text{if} \quad x > 0.33\ m, \end{cases} \qquad u(0,x,y) = 0\ m/s.$$

In Figure 10 we present the experimental and numerical results obtained at two different instants $t = 0.23\ s$ and $t = 0.46\ s$. Here, we display the bed profile, the water depth and the distribution of the sediments using the concentrations c_k, $k = 1,2,\ldots 10$. As the sediment is well distributed and the erosion rates are comparable, we do not observe ripple formation or any other effect of armoring, as the experimental results demonstrate in these results. The results obtained for this dam-break problem show that using a detailed description of sediments in the multilayer shallow water model, it is possible to accurately represent the vertical distribution of sediments constituting the bed. The proposed model perform very well for this case and its capture the correct flow and sediments structures without requiring complicated techniques or three-dimensional representations for the free-surface flows over erodible beds. For a better insight, we depict in Figure 11 the bed profile B and the averaged concentration c for the experimental and numerical simulations at time $t = 0.46\ s$. There is a good agreement between the results obtained using the experimental setup and the multilayer shallow water model for both the bed and sediment concentration distributions. The FVC method performs well for this test example and produces highly accurate and stable numerical results using reasonably coarse meshes. In general the sediment and flow features for this dam-break problem are

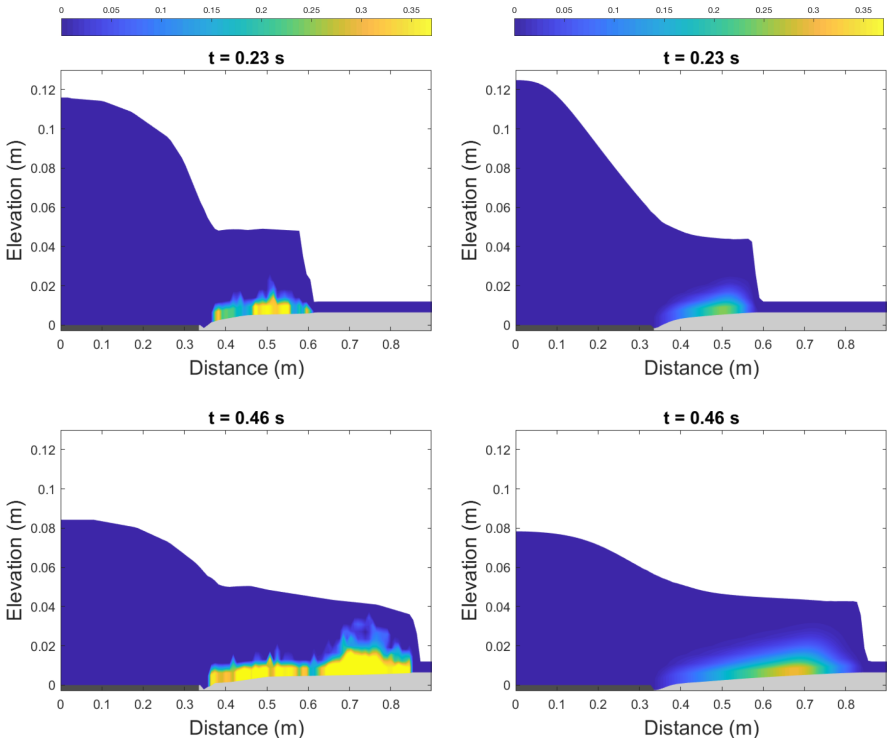

Fig. 10 Experimental results (first column) and numerical results (second column) obtained for the dam-break problem over an erodible bed at time $t = 0.23\ s$ (first row) and $t = 0.46\ s$ (second row).

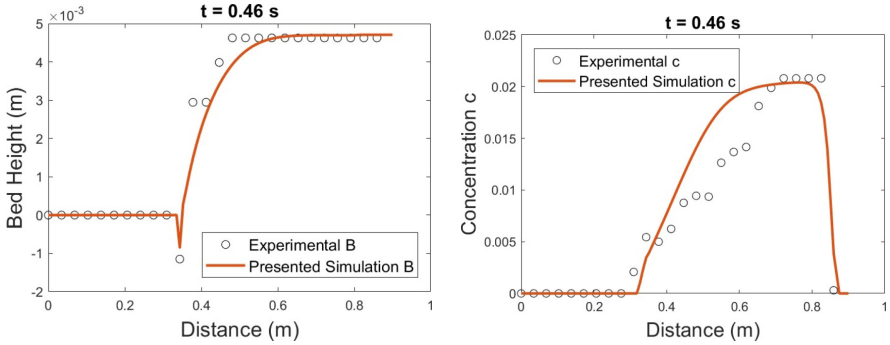

Fig. 11 Comparison between experimental and numerical results for the bed B (left) and the concentration c (right) obtained for the dam-break problem over an erodible bed at time $t = 0.46\ s$.

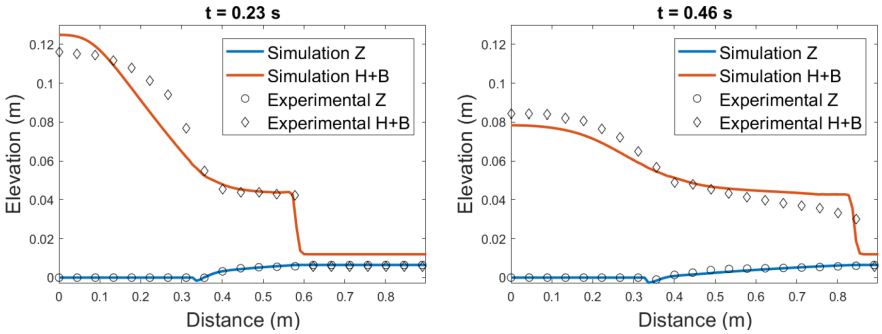

Fig. 12 Comparison between experimental and numerical results obtained for the dam-break problem over an erodible bed at time $t = 0.23\ s$ (first row) and $t = 0.46\ s$ (second row).

Table 2 Errors between the experimental and numerical results obtained for the bed, water height and averaged concentration at four different times $t = 0.12\ s, 0.24\ s, 0.35\ s$ and $0.46\ s$.

	B		H		c	
$t\ [s]$	L^2-error	L^∞-error	L^2-error	L^∞-error	L^2-error	L^∞-error
0.12	1.34E-06	1.69E-04	2.14E-03	3.592=E-02	4.25E-02	1.82E-01
0.24	4.22E-06	7.73E-04	1.33E-03	2.07E-02	1.09E-01	1.72E-01
0.35	5.76E-06	9.52E-04	7.23E-04	1.36E-02	1.85E-01	2.12E-01
0.46	8.74E-06	1.58E-03	6.95E-04	1.13E-02	4.72E-01	2.23E-01

computed with no numerical artifacts or spurious oscillations. According to these results the stability and shock capturing abilities of the FVC method are validated.

In Figure 12, we further compare the experimental and numerical results for this dam-break problem over an erodible bed. Here, we plot the profiles of the bed and water depth at two different times $t = 0.23\ s$ and $t = 0.46\ s$. The dam collapses at $t = 0$ and the flow system develops a shock wave heading downstream and a rarefaction wave traveling upstream. This is shown, in line with other experiments of this type, in Figure 12. Furthermore, no localized undershoots or overshoots were detected in either the flow velocity or the sediment concentration, even in the presence of steep gradients detected during the simulation. The results obtained for the sediment concentrations shown in Figure 10 illustrate the sedimentary diffusion and profiles of the sediment concentration can clearly be seen diffusing up through the layers. The proposed FVC method accurately approximates the solution to this dam-break problem over the erodible bed. Our final concern with this dam-break problem is to quantify the errors on the obtained experimental and numerical results. To this end, we present in Table 2, values of the L^2-error and L^∞-error between the experimental and numerical results obtained for the bed B, water height H and averaged concentration c evaluated at four different times $t = 0.12\ s$, $0.24\ s$, $0.35\ s$ and $0.46\ s$. Under the considered sediment conditions and for all times, the errors in the sediment concentration are larger than those obtained for the bed and the water

height. There is relatively low level of errors in our numerical simulations which is deeply encouraging for the multilayer shallow water model proposed in this study. To the knowledge of the authors, this is the first time that sediment concentration has been computed and compared to a simulation in both the vertical and horizontal dimensions for a dam-break problem.

6 Conclusions

A new class of experimental and numerical methods is presented in this study for the vertical distribution of sediments in dam-break flows. The experimental tools employ a high-speed camera and image processing toolbox to extract the concentration data for sediment transport. This new approach allows for the vertical distribution of sediments in a flow to be accurately and efficiently assessed. These techniques have been combined with a novel experimental setup that enable a small scale dam-break to be investigated. Fine sand has been used in the experimental study and measurements have been collected for its vertical distribution in the dam-break problem. Through the development of this model, multilayer shallow water equations and sediment transport equations (including erosion and deposition terms) have been coupled and considered. Mass exchange terms are accounted for in the inter-layered coupling for both water flow and sediment transport as well as including the vertical sediment diffusion. In order to solve the coupled system, the finite volume characteristics method was implemented along with a second-order splitting procedure to account for the source terms. The finite volume characteristics method is second-order accurate and encompasses a predictor-corrector type procedure in two stages. Firstly, the method reconstructs the numerical fluxes using the method of characteristics. This results in an upwind discretization of the characteristic variables and avoids the computation of the Riemann problem. Secondly, the solution is updated using the finite volume discretization of the conservation system. The method combines the desirable qualities of the finite volume discretization and the method of characteristics to create a simple solver for multilayer shallow water flows over erodible beds. In future work it is expected to extend this method from two-dimensional models in order to model a wider range of problems. It is also expected to include the effects of turbulence in both flow fields and sediment transport.

The collected experimental data was used for comparisons to the numerical results obtained using the proposed multilayer shallow water model. The results have also used for validations with numerical results obtained using the three-dimensional Navier-Stokes solver on the OpenFOAM software for a dam-break problem over a flat bed. These comparisons revealed very encouraging results for both the experimental method and the presented multilayer shallow water model. In additions, the proposed finite volume characteristics method exhibited good shape, high accuracy and stability behavior for all sediment transport regimes considered. The experimental method is low cost and easily replicable with great promise in being adaptable to efficiently assess more complex problems like composite beds. The

presented results demonstrate the capability of the multilayer models that can provide insight to complex suspended sediments and bed-load transport in dam-break flows. Further work in this research field should include composite beds in multiphase flows as well as particle tracking for the vertical distribution of sediments in dam-break flows. It is anticipated to use multiple cameras and composite images in the future to provide three-dimensional data and sediment capture.

References

1. Abderrezzak, K., Moran, A., Tassi, P., Ata, R., Hervouet, J.: Modelling river bank erosion using a 2D depth-averaged numerical model of flow and non-cohesive, non-uniform sediment transport. Advances in Water Resources **93**, 75–88 (2015)
2. Audusse, E., Benkhaldoun, F., Saida, S., Seaid, M., Tassi, P.: A fast finite volume solver for multi-layered shallow water flows with mass exchange. Journal of Computational Physics **272**, 23–45 (2014)
3. Audusse, E., Bristeau, M., Pelanti, M., Sainte-Marie, J.: Approximation of the hydrostatic Navier-Stokes system for density stratified flows by a multilayer model: Kinetic interpretation and numerical solution,. J. Comput. Phys. **230**, 3453–3478 (2011)
4. Audusse, E., Bristeau, M., Perthame, B., Sainte-Marie, J.: A multilayer Saint-Venant system with mass exchanges for Shallow Water flows. Derivation and Numerical Validation. M2AN Math. Model. Numer. Anal. **45**, 169–200 (2009)
5. Benkhaldoun, F., Sari, S., Seaid, M.: A flux-limiter method for dam-break flows over erodible sediment beds. Applied Mathematical Modelling **36**, 4847–4861 (2012)
6. Benkhaldoun, F., Seaid, M.: A simple finite volume method for the Shallow Water equations. J. Comp. Applied Math. **234**, 58–72 (2010)
7. Bijker, E.: Some considerations about scales for coastal models with movable bed. Delft Hydraulics Laboratory **50**, 1–128 (1967)
8. Brownlie, W.: Prediction of flow depth and sediment discharge in open channels. Report Number KH-R-43A. Keck Laboratory of Hydraulics and Water Resources, California Institute of Technology (1981)
9. Cao, Z., Carling, P.: Mathematical modelling of alluvial rivers: reality and myth. Part 1: General overview. Water Maritime Engineering **154**, 207–220 (2002)
10. Cao, Z., Pender, G., Wallis, S., Carling, P.: Computational Dam-Break Hydraulics over Erodible Sediment Bed. Journal of Hydraulic Engineering **67**, 149–152 (2004)
11. Capart, H., Young, D.: Formation of jump by the dam-break wave over a granular bed. Journal of Fluid Mechanics **372**, 165 – 187 (1998)
12. Chumakova, L., Menzaque, F., Milewski, P., Rosales, R., Tabak, E., Turner, C.: Shear instability for stratified hydrostatic flows. Communications on Pure and Applied Mathematics **62**, 183–197 (2009)
13. Cunge, J., Holly, F., Verwey, A.: Practical Aspects of Computation River Hydraulics. Pitman Publishing Inc. Boston (2002)
14. Dawei, S., Weibing, F.: A Two-Dimensional Numerical Model of Suspended Sediment Transport Using in the Radial Sand Ridge Field. International Conference on Mechatronic Science, Electric Engineering and Computer pp. 826–830 (2011)
15. Dyke, P.: Modeling Coastal and Offshore Processes (2007)
16. Einstein, H.: Formulas for the Transportation of Bed Load. Transactions of the American Society of Civil Engineers **107**, 561–573 (1949)
17. El-Amrani, M., Seaid, M.: Numerical simulation of natural and mixed convection flows by Galerkin-characteristic method. Int. J. Numer. Meth. Fluids. **53**(12), 1819–1845 (2007)
18. Fernández-Nieto, E., Koné, E., Chacón, T.: A Multilayer Method for the Hydrostatic Navier-Stokes Equations: A Particular Weak Solution. J. Sci. Comput. **57**, 1–30 (2013)

19. Grass, A.: Sediment Transport by Waves and Currents. SERC London Cent. Mar. Technol. (FL29) (1981)
20. Gula, J., Zeitlin, V., Bouchut, F.: Instabilities of buoyancy-driven coastal currents and their nonlinear evolution in the two-layer rotating shallow water model. Part 2. Active lower layer. J. Fluid Mechanics. **665**, 209–237 (2010)
21. Huang, S., Sun, Z., Xu, D., Xia, S.: Vertical distribution of sediment concentration. Journal of Zhejiang University SCIENCE **9**, 1560– (2008)
22. Kubatko, E., Westerink, J.: Exact discontinuous solutions of Exner's bed evolution model: Simple theory for sediment bores. Journal of Hydraulic Engineering **133** (2007)
23. Liu, X., Beljadid, A.: A coupled numerical model for water flow, sediment transport and bed erosion. Computers and Fluids **154**, 273–284 (2017)
24. Meyer-Peter, E., Müller, R.: Formulas for Bed-Load Transport. Report on 2nd meeting on International Association on Hydraulic Structures Research pp. 39–64 (1948)
25. Paphitis, D.: Sediment movement under unidirectional flows: An assessment of empirical threshold curves. Coastal Engineering **43**, 227–245 (2001)
26. Rahuel, J., Holly et al., F.: Modeling of Riverbed Evolution for Bedload Sediment Mixtures. J. of Hydr. Engrg **11**, 1521–1542 (2016)
27. Rahuel, J., Holly, F., Holly Chollet, J., Yang, G.: Modeling of Riverbed Evolution for Bedload Sediment Mixtures. Journal of Hydraulic Engineering **115** (1989)
28. Rehman, K., Cho, Y.: Bed Evolution under Rapidly Varying Flows by a New Method for Wave Speed Estimation. Journal of Computational Physics **43**, 357–372 (2016)
29. van Rijn, L.: Sediment pick-up functions. Journal of Hydraulic Engineering **110**, 1494–1502 (1984)
30. van Rijn, L.: Unified View of Sediment Transport by Currents and Waves. I : Initiation of Motion, Bed Roughness, and Bed-Load Transport. Journal of Hydraulic Engineering **113**, 649–667 (2007)
31. Rowan, T., Seaid, M.: Efficient computational models for shallow water flows over multilayer erodible beds. Engineering Computations **37**, 401–429 (2019)
32. Rowan, T., Seaid, M.: Two-dimensional numerical modelling of shallow water flows over multilayer movable beds. Applied Mathematical Modelling **88**, 474–497 (2020)
33. Rubey, W.: Settling velocity of gravel, sand, and silt particles. American Journal of Science **148**, 325–338 (1933)
34. Shields, A.: Anwendung der Ahnlichkeitsmechanik und der Turbulenzforschung auf die Geschiebebewegung. Mitteilung der preussischen Versuchsanstalt fur Wasserbau und Schiffbau **26** (1936)
35. Shu, C.: Total Variation Diminishing Time Discretizations. SIAM J. Sci. Stat. Comput. **9**, 1073–1084 (1988)
36. Soares-Frazao, S., et al: Dam-break flows over mobile beds: Experiments and benchmark tests for numerical models. Journal of Hydraulic Research **50**, 364–375 (2012)
37. Strang, G.: On the construction and the comparison of difference schemes. SIAM J. Numer. Anal. **5**, 506–517 (1968)
38. Terzaghi, K., Peck, R., Mersi, G.: Soil Mechanics in Engineering Practice. John Wile and Sons Publishers (1996)
39. Vercruysse, K., Grabowski, R., Rickson, R.: Suspended sediment transport dynamics in rivers: Multi-scale drivers of temporal variation. Earth-Science Reviews **166**, 38–52 (2017)
40. Wu, W.: Depth-averaged two-dimensional numerical modeling of unsteady flow and nonuniform sediment transport in open channels. J. Hydraul. Eng. - ACSE **130**, 1013–1024 (2004)
41. Wu, W., Vieira, D.: One-dimensional channel network model CCHE1D 2.0. National Center for Computational Hydroscience and Engineering (2002)
42. Wu, W., Wang, S.: Formulas for Sediment Porosity and Settling Velocity. Journal of Hydraulic Engineering **132**, 858–862 (2006)
43. Yang, Z., Zou, Z., Xue, W., Sun, D.: Experimental study of near-bed concentration and sediment vertical mixing parameter for vertical concentration distribution in the surf zone. International Journal of Sediment Research **35**, 27–41 (2020)